

Chapter 6

Theory and Experiments for a Practical Usecase



6.1 The Problem of Landing and Takeoff On/from a Sloped Surface

In many aerial robot applications such as search and rescue, the task consists on providing assistance in hostile environments such as mountains or civil areas after natural catastrophes. In this scenarios it is very likely that the terrain is not flat, making the landing and takeoff maneuvers of the aerial robot very complicate and unsafe.

The problem of landing on a sloped (not flat) surface is a very challenging problem for an unidirectional-thrust aerial vehicle due to its underactuation. In fact, the task requires to control both position and attitude since the vehicle has to be oriented as the surface on which we want to land, but this is not possible. It is well known that one can control the position of an unidirectional-thrust aerial vehicle, but not its attitude. The latter is indeed a byproduct of the particular position trajectory that we want to follow (given by the differential flatness). The classical approach for free-flying vehicles is based on motion planning [1–3] (sometimes called *perching* maneuver). It consists on exploiting the flatness of the system with respect to the position [4] to plan a desired trajectory such that the vehicle ends the maneuver with the proper position and orientation. Different controllers can be then applied to track this trajectory. However, the success of the maneuver requires an almost perfect tracking that implies an almost perfect state estimation and knowledge of the model. Otherwise, small deviations from the nominal trajectory would lead to miss the target or to crash on it.

On the other hand, we shall show that the use of a tether is very useful to solve the faced problem of landing and takeoff on a sloped surface. As we saw in Chap. 4, for a tethered aerial vehicle we have the great advantage to partially control the attitude of the vehicle. Under certain conditions better stated in the following, this property

allows to perform the landing and takeoff maneuvers in a very reliable way, even in the presence of model errors, and for almost any sloped surface.

In Chaps. 4 and 5, we already showed the case of a tether aerial vehicle, together with an actuated link, landing and taking off on/from a flat moving surfaces. Nevertheless, this configuration requires to add an actuator that increases the complexity of the system and reduces its already limited payload if placed on-board. For these reasons, to increase the applicability of the method to solve the sought problem, we instead consider the case of a passive tether that does not require extra actuation. We remark that the results found in Chap. 4 are still valid. The only difference is that the link length is now not controllable but remains constant.

One of the main contributions of our work is the definition of some general conditions to perform a robust takeoff and landing. We then provide a careful analysis and a comparison of the contact-free flight and passive-tethered methods, based on these conditions. This study shows that, when an anchoring spot is available, the tether solution is highly preferable with respect to the contact-free flight one since it is the only one that allows to land on any sloped surface, and with good repeatability and robustness to tracking inaccuracies. Focusing on the passive-tether solution, in order to execute the maneuver respecting the inputs limits and to increase the robustness and safety of the maneuver, we also design a planner to compute an optimal reference trajectory. The latter is then followed by the hierarchical controller Γ_{HC}^b for the output y^b (see Sect. 4.5). We chose this controller rather than one based on dynamic feedback linearization, Γ_{DFL}^b , because highly dynamic trajectory are not required for the task (to increase the safety of the maneuver). The global method is finally tested through exhaustive real experiments in which a quadrotor is able to perform the landing and takeoff on/from a sloped surface tilted by an angle up to 60° . Part of the following results have been published in [5, 6].

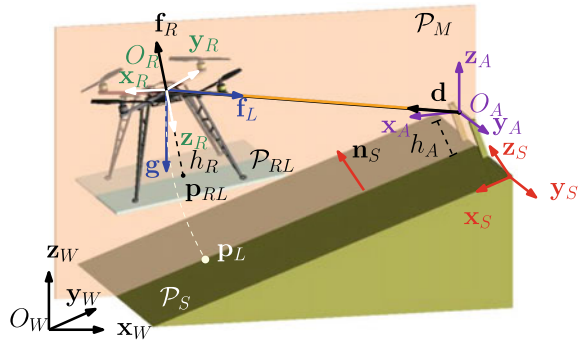
6.2 Modeling

The unidirectional-thrust aerial vehicle is modeled as in Sect. 4.3 (link attached to a fixed platform and with a fixed length, i.e., no link actuator) and its states and control inputs are described by the same variables. We assume the vehicle equipped with at least three landers whose ending parts form the *landers plane* \mathcal{P}_{RL} . As in the most common case in reality, we assume \mathbf{z}_R perpendicular to \mathcal{P}_{RL} .¹ Then we define $\mathbf{p}_{RL} \in \mathbb{R}^3$ as the projection of \mathbf{p}_R on \mathcal{P}_{RL} and $h_R = \|\mathbf{p}_R - \mathbf{p}_{RL}\|$ as the distance between \mathbf{p}_R and \mathcal{P}_{RL} .

We assume that the *landing/takeoff (LTO) surface* is planar in the neighborhood of the desired landing point and it is defined by $\mathcal{P}_S := \{\mathbf{p} = [x \ y \ z]^\top \in \mathbb{R}^3 \mid ax + by + cz + d = 0\}$ where $a, b, c, d \in \mathbb{R}$ are the parameters of the plane. In particular, $\mathbf{n}_S = (1/\sqrt{a^2 + b^2 + c^2})[a \ b \ c]^\top$ are the coordinates in \mathcal{F}_W of the unit vector normal to \mathcal{P}_S . Then we define a frame \mathcal{F}_S that is rigidly attached to

¹The equal interesting but unusual case of an arbitrary \mathcal{P}_{RL} is left as future work.

Fig. 6.1 Representation of the system and its main variables. © 2020 IEEE. Reprinted, with permission, from [5]



\mathcal{P}_S , whose axes are $\{\mathbf{x}_S, \mathbf{y}_S, \mathbf{z}_S\}$. If $\mathbf{n}_S = \mathbf{z}_W$, i.e., \mathcal{P}_S is horizontal, then we set $\{\mathbf{x}_S, \mathbf{y}_S, \mathbf{z}_S\} = \{\mathbf{x}_W, \mathbf{y}_W, \mathbf{z}_W\}$. In the others (more interesting) cases, i.e., when \mathcal{P}_S is locally inclined, the axes of \mathcal{F}_S are set as: $\mathbf{z}_S = \mathbf{n}_S$, $\mathbf{y}_S = (\mathbf{z}_W \times \mathbf{z}_S) / \|\mathbf{z}_W \times \mathbf{z}_S\|$ and $\mathbf{x}_S = (\mathbf{y}_S \times \mathbf{z}_S) / \|\mathbf{y}_S \times \mathbf{z}_S\|$. The origin of \mathcal{F}_S , O_S , is taken as any arbitrary position on \mathcal{P}_S . Figure 6.1 gives a schematic representation of the whole system.

6.2.1 Model in Free (Non-tethered) Flight

Recalling the modeling of a unidirectional-thrust aerial vehicle in contact-free flight done in Sect. 3.2, its configuration is described by \mathbf{p}_R and \mathbf{R}_R and its dynamic is given by:

$$m_R \ddot{\mathbf{p}}_R = -m_R g \mathbf{z}_W - f_R \mathbf{z}_R \quad (6.1)$$

$$\mathbf{J}_R \dot{\boldsymbol{\omega}}_R = \mathbf{J}_R \boldsymbol{\omega}_R \times \boldsymbol{\omega}_R + \boldsymbol{\tau}_R. \quad (6.2)$$

Model (6.1) holds as long as the aerial vehicle is not in contact with the surface. In this last case, i.e., $\mathcal{P}_{RL} \equiv \mathcal{P}_S$, (6.1) has to be extended taking into account the reaction force of the surface, denoted by $f_N \in \mathbb{R}$, and the static friction force, denoted by $\mathbf{f}_S \in \mathbb{R}^3$, thus obtaining:

$$m_R \ddot{\mathbf{p}}_R = -m_R g \mathbf{z}_W - f_R \mathbf{z}_R + f_N \mathbf{n}_S + \mathbf{f}_S, \quad (6.3)$$

where $f_N \geq \underline{f}_N$, $\mathbf{z}_S^\top \mathbf{f}_S = 0$ and $\|\mathbf{f}_S\| \leq \overline{f}_S$. For a standard surface $\underline{f}_N = 0$ and $\overline{f}_S = \mu f_N$ where $\mu \in \mathbb{R}_{\geq 0}$ is the characteristic friction coefficient of the contact between \mathcal{P}_{RL} and \mathcal{P}_S . If \mathcal{P}_{RL} and \mathcal{P}_S are equipped with an adhesive membrane (e.g., a Velcro or a gecko inspired material) then $\underline{f}_N \in \mathbb{R}_{\leq 0}$ is the maximum negative reaction force. In these cases both \underline{f}_N and \overline{f}_S depend on the adhesive membrane.

6.2.2 Model in Tethered Flight

Let us consider one of the particular tethered aerial cases considered in Sect. 4.3. In particular we consider an aerial vehicle tethered to a fixed point through a constant-length link, such as a cable or a chain. One end of the link is attached to the aerial vehicle at O_R through a passive 3D spherical joint and the other end is attached to an *anchor point* O_A rigidly attached to the surface. The position of O_A is described by $\mathbf{p}_A \in \mathbb{R}^3$ in \mathcal{F}_W and its distance from \mathcal{P}_S is given by $h_A = \mathbf{z}_S^\top (\mathbf{p}_A - \mathbf{p}_L) \in \mathbb{R}_{\geq 0}$, $\forall \mathbf{p}_L \in \mathcal{P}_S$.

When the link is slack and the aerial vehicle is not in contact with the LTO surface the dynamic model of the system is given by (6.1)–(6.2).

On the other hand, when the link is taut, the system model is the one presented in Sect. 4.3 when the link length is constant. We recall that $\mathbf{p}_R \in \mathcal{S}_l(\mathbf{p}_A) = \{\mathbf{p} \in \mathbb{R}^3 \mid \mathbf{p} = \mathbf{p}_A + l\mathbf{d}, \forall \mathbf{d} \in \mathbf{S}^2\}$, where $\mathcal{S}_l(\mathbf{p}_A)$ is a sphere of radius l centered on \mathbf{p}_A , and \mathbf{d} is the unit vector that represents the attitude of the link expressed in \mathcal{F}_W .

We introduce the frame $\mathcal{F}_A = \{O_A, \mathbf{x}_A, \mathbf{y}_A, \mathbf{z}_A\}$ defined as $\mathbf{z}_A = \mathbf{z}_W$, $\mathbf{y}_A = \mathbf{y}_S$ and $\mathbf{x}_A = \mathbf{y}_A \times \mathbf{z}_A / \|\mathbf{y}_A \times \mathbf{z}_A\|$. Recalling the modeling of Sect. 4.3 and assuming $\mathcal{F}_C = \mathcal{F}_A$, we have that the dynamics of the system is equal to (4.3) and (4.11) for the rotational and translational part, respectively. We recall that the model can be easily derived from (4.10) considering only the first three row, $\dot{l} = \ddot{l} = 0$ and replacing the notation C with the notation A where appropriate. For the reader convenience we report here the main equations with the proper notation that will be useful also in the following.

The vector \mathbf{d}^A denotes the expression of \mathbf{d} in \mathcal{F}_A . It is parametrized by the *elevation angle*, $\varphi \in [0, 2\pi]$, and the *azimuth angle*, $\delta \in [-\frac{\pi}{2}, \frac{\pi}{2}]$, such that $\mathbf{d}^A = [\cos \delta \cos \varphi \quad -\sin \delta \quad \cos \delta \sin \varphi]^\top$. Since the link is attached to O_R , the rotational dynamics of the vehicle is independent of the translational one and it is equal to (6.2). We retrieve the dynamics of² $\mathbf{q} = [\varphi \quad \delta]^\top$ with the Newton–Euler method applying the balance of forces at O_R :

$$m_R \ddot{\mathbf{p}}_R = -m_R g \mathbf{z}_W - f_R \mathbf{z}_R - f_L \mathbf{d}, \quad (6.4)$$

where $\ddot{\mathbf{p}}_R$ is obtained differentiating twice $\mathbf{p}_R = \mathbf{p}_A + l\mathbf{R}_A \mathbf{d}^A$:

$$\ddot{\mathbf{p}}_R = \mathbf{R}_A (\mathbf{J}_q \dot{\mathbf{q}} + \mathbf{J}_q \ddot{\mathbf{q}}), \quad \mathbf{J}_q = \begin{bmatrix} -l \cos \delta \sin \varphi & -l \cos \varphi \sin \delta \\ 0 & -l \cos \delta \\ l \cos \delta \cos \varphi & -l \sin \delta \sin \varphi \end{bmatrix},$$

where $\mathbf{R}_A \in \mathbb{R}^{3 \times 3}$ is the rotation matrix from \mathcal{F}_A to \mathcal{F}_W . Equations (6.2) and (6.4) fully describe the dynamics of the system when the link is taut.

²In this chapter, since the length of the link is constant, l is not a generalized variable but becomes a parameter of the system.

Similarly to the non-tethered case, when the robot is tethered and in contact with the surface, the model (6.4) is extended taking into account the reaction and friction forces, $f_N \in \mathbb{R}$ and $f_S \in \mathbb{R}$, respectively:

$$m_R \ddot{\mathbf{p}}_R = -m_R g \mathbf{z}_W - f_R \mathbf{z}_R - f_L \mathbf{d} + f_N \mathbf{n}_S + \mathbf{f}_S. \quad (6.5)$$

6.3 Conditions for Robust Landing and Takeoff

In the following we define and analyze the problem of landing on \mathcal{P}_S at a *desired landing position* $\mathbf{p}_L^* \in \mathcal{P}_S$. Analogous conditions can be drawn for the takeoff problem, which are omitted here for brevity. Denoting with $t_L \in \mathbb{R}_{>0}$ the *landing time*, a correct and robust landing is such if the following conditions are satisfied:

- (1) \mathbf{p}_{RL} converges to \mathbf{p}_L^* , i.e., $\mathbf{p}_{RL}(t_L) = \mathbf{p}_L^* \in \mathcal{P}_S$;
- (2) the robot orientation has to be such that \mathcal{P}_{RL} and \mathcal{P}_S are parallel, i.e., $\mathbf{z}_R(t_L) = \mathbf{z}_R^* = -\mathbf{z}_S$, in order to have the robot perfectly in contact with the surface;
- (3) the vehicle has to reach this configuration with almost zero kinetic energy in order to avoid hard impacts, i.e., at time t_L^- , immediately before of touching the surface, it has to be that $\dot{\mathbf{p}}_R(t_L^-) = \mathbf{0}$ and $\boldsymbol{\omega}_R(t_L^-) = \mathbf{0}$;
- (4) all the accelerations should be also zero at t_L^- , i.e., $\ddot{\mathbf{p}}_R(t_L^-) = \mathbf{0}$ and $\dot{\boldsymbol{\omega}}_R(t_L^-) = \mathbf{0}$, thus obtaining a smooth and gentle maneuver;

Definition (Inclined hovering) The system is said in *inclined hovering* if $\mathbf{z}_R \neq -\mathbf{z}_W$ and Conditions (3), and (4) coexist. \square

- (5) after the conclusion of the landing maneuver, at time t_L^+ , when the robot is in contact with the surface, \mathbf{p}_L^* has to be a stable position, i.e., zero velocity and acceleration. This condition prevents the robot to fly away from the surface or to slide down on it when the motors are switched off after the landing maneuver.

Remark At time t_L^- the robot is not yet in contact with the surface and the flying model has to be used to describe the system (Eqs. (6.1), (6.2) or (6.4), (6.2)). On the contrary, at time t_L^+ the vehicle is in contact with the surface thus Eqs. (6.3) or (6.5) have to be used. \square

Notice that the Condition (4), although not strictly necessary, lets the vehicle approach the surface in a static equilibrium condition, passing from flight to contact very smoothly and in a more robust way with respect to model uncertainties.

If, due to the characteristics of the system, Condition (4) is not attainable, the landing can still be done but when at time t_L^+ the vehicle touches the surface, one has to find the way (e.g., turning off the motors as quickly as possible and using a Velcro system) to immediately pass in a stable condition in order to remain in contact with the surface without flying away or sliding on it (Condition (5)). Nevertheless, this could be not possible for some surfaces without the use of a tether or a Velcro-like solution.

Remark For the takeoff, only Condition (5), that now is an initial condition, has to be fulfilled. \square

6.4 Analysis and Comparison for Landing and Takeoff

In the following we analyze two different kind of approaches for the landing: the free-flying and the tethered maneuvers. For both cases we define the conditions to satisfy the landing objectives and illustrate the benefits of the tethered solution.

6.4.1 Contact-Free Flight Method

Replacing the conditions $\mathbf{z}_S = \mathbf{z}_W$ and $\ddot{\mathbf{p}}_R(t_L^-) = \mathbf{0}$ in (6.1), it is clear that the only case in which Condition (4) holds is when \mathcal{P}_S is horizontal. In all the other cases $\ddot{\mathbf{p}}_R(t_L^-) \neq \mathbf{0}$, which means that the aerial vehicle cannot approach the surface in a fully stable condition.

For the Condition (5), imposing $\ddot{\mathbf{p}}_R(t_L^+) = \mathbf{0}$ in (6.3) and projecting the two sides of (6.3) on \mathcal{F}_S , we obtain

$$f_N = m_R g \mathbf{z}_S^\top \mathbf{z}_W + f_R, \quad \mathbf{x}_S^\top \mathbf{f}_S = m_R g \mathbf{x}_S^\top \mathbf{z}_W, \quad \mathbf{y}_S^\top \mathbf{f}_S = 0. \quad (6.6)$$

The first two conditions of (6.6) let us determine which is the maximum thrust at time t_L^+ and the maximum slope to have Condition (5) fulfilled, i.e.:

$$f_R(t_L^+) \leq m_R g \mathbf{z}_S^\top \mathbf{z}_W - \underline{f}_N \quad \text{and} \quad \mathbf{x}_S^\top \mathbf{z}_W \leq \overline{f}_S / (m_R g). \quad (6.7)$$

Thus, one can land on any point of \mathcal{P}_S only if (6.7) holds, restricting the set of admissible slopes.

Assuming that the surface fulfills (6.7), we now investigate how to reach it, and in particular, how to achieve the first three conditions. In the less interesting case of a horizontal surface, one can simply follow a trajectory along \mathbf{z}_W in hovering condition to reach \mathbf{p}_L^* with zero velocities and accelerations. In the more interesting case of a sloped surface, this is a very challenging problem due to the underactuation of the vehicle. From the theory it is well known that the system is differentially flat with respect to \mathbf{p}_R and the rotation around \mathbf{z}_R [4]. Therefore one can track any desired position trajectory, $\mathbf{p}_R^d(t)$, such that $\mathbf{p}_{RL}(t_L) = \mathbf{p}_L^*$ and $\dot{\mathbf{p}}_R(t_L^-) = \mathbf{0}$, but the orientation of the vehicle along the trajectory is exactly determined by $\mathbf{p}_R^d(t)$ and its derivatives. Thus it is not possible to control the attitude independently from the position trajectory. The classical method to overcome this issue is to use a state-to-state planner like, e.g., the ones presented in [3] slightly modified, that gives a particular position trajectory $\mathbf{p}_R^d(t)$ that satisfies Conditions (1), (2) and (3).

Remark Consider an aerial vehicle that has to land on a given surface \mathcal{P}_S , at any desired point $\mathbf{p}_L^* \in \mathcal{P}_S$. If the landing has to be performed using a contact-free flight method then, in general:

- if \mathcal{P}_S is non-horizontal then Conditions (1), (2), (3) can only be achieved by a very accurate tracking of a perfectly synchronized dynamic maneuver generated using a state-to-state kino-dynamic planner;
- Condition (5) is fulfilled iff $f_R(t_L^+)$ and \mathcal{P}_S are such that the two conditions in (6.7) hold;
- Condition (4) is fulfilled iff \mathcal{P}_S is horizontal; □

Assuming that the non-easy motion planning problem is solved, one could use different types of controllers, as the ones in [1, 7], to track the planned trajectory. Nevertheless, these methods lack in general of robustness since small tracking errors could lead, e.g., to miss the target or to crash on it if the velocity is not well tracked. Furthermore, a precise model and an accurate and high-rate state estimation are needed.

To partially solve those problems and the ones related to the sliding, a common practical solution is to use a Velcro, as in [2, 8], to help the perching. However these solutions are not feasible in a real environments. Velcro solution also does not permit to easily takeoff after the perching.

6.4.2 Tethered Method

In this section we show that the tethered method overcomes the limits of contact-free flight (in particular the impossibility to satisfy Condition (4) for sloped surfaces, which guaranties a safer landing maneuver) thanks to the inclined equilibria.

For the tethered method the landing position must belong to $\mathcal{S}_l(\mathbf{p}_A) \cap \mathcal{P}_S$. We then first investigate which are the points in this set that satisfy Condition (4). Consider a generic point $\mathbf{p}_L \in \mathcal{S}_l(\mathbf{p}_A) \cap \mathcal{P}_S$. From simple geometry we have

$$\mathbf{d} = (\mathbf{p}_L - \mathbf{p}_A + h_R \mathbf{z}_S) / l. \quad (6.8)$$

Since \mathbf{p}_A , l and h_R are given parameters, finding the \mathbf{p}_L that satisfies Condition (4) is equivalent to find the \mathbf{d} that satisfies the same condition. Projecting both sides of (6.8) on \mathbf{z}_S^\top we obtain

$$\mathbf{z}_S^\top \mathbf{d} = (h_R + \mathbf{z}_S^\top (\mathbf{p}_L - \mathbf{p}_A)) / l = (h_R - h_A) / l := c. \quad (6.9)$$

Then, in order to fulfill Condition (4), let us project both sides of (6.4) on the plane $\{\mathbf{x}_S, \mathbf{y}_S\}$, and set $\ddot{\mathbf{p}}_R = \mathbf{0}$, thus obtaining

$$f_L \mathbf{P}_{xy}^S \mathbf{d} = -m_R g \mathbf{P}_{xy}^S \mathbf{z}_W, \quad (6.10)$$

where $\mathbf{P}_{xy}^S = [\mathbf{x}_S \ \mathbf{y}_S]^\top$. Equation (6.10) implies that $\mathbf{P}_{xy}^S \mathbf{d}$ is parallel to $\mathbf{P}_{xy}^S \mathbf{z}_W$. Since $f_L \geq 0$ and $m_R g > 0$, we obtain

$$(\mathbf{P}_{xy}^S \mathbf{d}) / \|\mathbf{P}_{xy}^S \mathbf{d}\| = -(\mathbf{P}_{xy}^S \mathbf{z}_W) / \|\mathbf{P}_{xy}^S \mathbf{z}_W\| = [1 \ 0]^\top =: \mathbf{z}_W^{S_{xy}}. \quad (6.11)$$

Notice that (6.11) requires³ $\|\mathbf{P}_{xy}^S \mathbf{z}_W\| \neq 0$ and $\|\mathbf{P}_{xy}^S \mathbf{d}\| \neq 0$. The latter inequality implies also that $(h_R - h_A) \neq l$. From (6.9) and (6.11) and applying some simple geometry we obtain

$$\mathbf{d} = [\mathbf{x}_S \ \mathbf{y}_S \ \mathbf{z}_S] \begin{bmatrix} \sqrt{1-c^2} & 0 & c \end{bmatrix}^\top =: \tilde{\mathbf{d}}, \quad (6.12)$$

where $\tilde{\mathbf{d}}$ is defined as the (unique) \mathbf{d} for which Condition (4) is fulfilled. This proves that, given the parameters of the system, \mathbf{p}_A , l and h_R , it exists a (unique) $\tilde{\mathbf{p}}_L = \mathbf{p}_A + l\tilde{\mathbf{d}} - h_R \mathbf{z}_S$, for which Condition (4) is respected.

Remark The use of a tether creates the conditions to approach or depart from a sloped surface in a stable equilibria condition (*inclined hovering*), i.e., in a more robust and safer way. In fact, using the tether it exists a landing position in which one can land in *inclined hovering* for *any* sloped surface (in contact-free flight this position exists *only* for horizontal surfaces). Moreover, given any desired landing position $\mathbf{p}_L^* \in \mathcal{P}_S$, one can always fulfill Condition (4) setting $h_A \neq h_R - l$ and

$$\mathbf{p}_A = \mathbf{p}_L^* + h_R \mathbf{z}_S - l\tilde{\mathbf{d}} := \tilde{\mathbf{p}}_A. \quad (6.13)$$

□

6.4.2.1 Compliance with Condition (5)

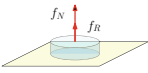
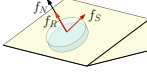
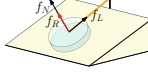
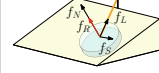
If $(\mathbf{x}_S^\top \mathbf{z}_W)(\mathbf{x}_S^\top \mathbf{d}) < 0$, i.e., if the landing spot is below the projection of \mathbf{p}_A on \mathcal{P}_S , then a solution of (6.5) for $\tilde{\mathbf{p}}_R(t_L^+) = \mathbf{0}$ is

$$\begin{aligned} f_L &= -\frac{m_R g \mathbf{x}_S^\top \mathbf{z}_W}{\mathbf{x}_S^\top \mathbf{d}}, \quad f_N = m_R g \mathbf{z}_S^\top \mathbf{z}_W - f_R + f_L \mathbf{z}_S^\top \mathbf{d}, \\ \mathbf{y}_S^\top \mathbf{f}_S &= f_L \mathbf{y}_S^\top \mathbf{d}, \quad \mathbf{x}_S^\top \mathbf{f}_S = 0. \end{aligned} \quad (6.14)$$

In this case the tension is always positive and, from the conditions on f_N and \mathbf{f}_S in (6.14), we can determine which is the maximum thrust intensity at time t_L^+ and the maximum slope of the surface to respect the Condition (5), i.e.,

³When $\|\mathbf{P}_{xy}^S \mathbf{z}_W\| = 0$ the surface is horizontal and any \mathbf{d} such that (6.9) holds, satisfies Condition (4). In this condition, one can still land with the tethered configuration keeping $f_L = 0$ and using the same method for contact-free flight.

Table 6.1 Characteristics of contact-free flight and tethered configuration for the landing problem. Analogous conditions hold for the take-off. © 2020 IEEE. Reprinted, with permission, from [5]

Method	Contact-free flight		Tethered flight	
Fulfillment of Condition	All	All but Condition (4) ($\dot{\mathbf{p}}_R(t_L^-) \neq \mathbf{0}$)	All	All but Condition (4) ($\dot{\mathbf{p}}_R(t_L^-) \neq \mathbf{0}$)
Surf. orientations	$\mathbf{z}_S = \mathbf{z}_W$	$\frac{\mathbf{x}_S^\top \mathbf{z}_W}{f_S / (m_R g)} \leq$	any	$\frac{ -m_R g \mathbf{y}_S^\top \mathbf{d}(\mathbf{x}_S^\top \mathbf{z}_W \mathbf{x}_S^\top \mathbf{d}) }{f_S} \leq$
Anchor positions	–	–	any	any
Landing positions	any	any	$\mathbf{p}_L = \mathbf{p}_A + l\tilde{\mathbf{d}} - h_R \mathbf{z}_S$	$\mathbf{p}_L \in \mathcal{S}_l(\mathbf{p}_A) \cap \mathcal{P}_S$
Max. f_R at t_L^+	$f_R \leq m_R g - \underline{f}_N$	$f_R \leq m_R g \frac{\mathbf{x}_S^\top \mathbf{z}_W}{f_S} - \underline{f}_N$	$f_R(t_L^+) \leq \overline{f}_R$	$f_R(t_L^+) \leq \overline{f}_R$
				
Pros	Simple system		Possibility to perform the maneuver reaching a stable equilibria condition; a planner is not required; robustness to model uncertainties and tracking errors	
Conditions	Not feasible for every slope; it requires: a planner, high tracking accuracy, precise state estimation and knowledge of the model (very low robustness)		Need of a method to pass from contact-free flight condition to tethered one	

$$f_R(t_L^+) \leq m_R g \frac{\mathbf{x}_S^\top \mathbf{z}_W}{f_S} (1 - (\mathbf{z}_S^\top \mathbf{d} / \mathbf{x}_S^\top \mathbf{d})) - \underline{f}_N =: \overline{f}_R \quad (6.15)$$

$$|-m_R g \mathbf{y}_S^\top \mathbf{d}(\mathbf{x}_S^\top \mathbf{z}_W / \mathbf{x}_S^\top \mathbf{d})| \leq \overline{f}_S. \quad (6.16)$$

If $\mathbf{d} = \tilde{\mathbf{d}}$ then the Condition (6.16) holds for any surface. In the opposite case of $(\mathbf{x}_S^\top \mathbf{z}_W)(\mathbf{x}_S^\top \mathbf{d}) \geq 0$, i.e., when the landing spot is above the projection of \mathbf{p}_A on \mathcal{P}_S , we have that $f_L = 0$ and the conditions in (6.7) have to be respected.

Table 6.1 summarizes all the previous results. To accomplish Conditions (1), (2) and (3) the controllers Γ_{HC}^b or Γ_{DFL}^b presented in Sects. 4.5.2 and 4.6.2, respectively, can be used. Although not needed, to further improve the robustness and the reliability of the maneuver, we designed a motion planning method presented in the following Sect. 6.5 to optimize the motion during the landing and takeoff maneuvers. Notice that with the tethered method we can achieve all the landing conditions for any surface and any desired landing position by properly choosing the anchor point.

6.5 Optimal Trajectory Planning

Given the tracking controllers of Sects. 4.5.2 and 4.6.2 for the output \mathbf{y}^b , we need to design a feasible desired trajectory $\mathbf{y}^{bd}(t)$ that fulfills the objectives of Sect. 6.3 to successfully perform the landing. From now on we focus on the landing problem, since the trajectory for the takeoff can be computed with the same method.

We assume that in a preliminary phase the vehicle has been tethered to the anchor point \mathbf{p}_A such that $\mathbf{p}_L^* = \tilde{\mathbf{p}}_L$, and the system has been steered to the state \mathbf{x}_0 for which the link results taut. Then, the initial and final value of the trajectory, $\mathbf{y}^{bd}(t)$, has to be such that $\mathbf{x}(t_0) = \mathbf{x}_0$ and $\mathbf{x}(t_L) = \mathbf{x}^*$, where \mathbf{x}^* corresponds to the Conditions (1), (2), (3) and (4). In the following we define the final desired output value and an optimal planner to design a feasible and optimal trajectory that fulfills all the objectives of Sect. 6.3, and respects the input limits.

6.5.1 Final Desired Output

Since \mathbf{p}_{RL} and \mathbf{z}_R are independent from ψ , then ψ^* can be chosen arbitrarily. Given a desired landing position $\mathbf{p}_L^* \in \mathcal{S}_l(\mathbf{p}_A) \cap \mathcal{P}_S$, one can compute the corresponding desired link attitude \mathbf{d}^* from (6.8). Finally, from the parametrization of \mathbf{d} and (4.26) we can complete the remaining entries of the desired output \mathbf{y}^{b*} :

$$\begin{aligned}\varphi^* &= \text{atan2}\left(\mathbf{z}_A^\top \mathbf{d}^*, \mathbf{x}_A^\top \mathbf{d}^*\right) \\ \delta^* &= \text{atan2}\left(\mathbf{y}_A^\top \mathbf{d}^*, \sqrt{(\mathbf{z}_A^\top \mathbf{d}^*)^2 + (\mathbf{x}_A^\top \mathbf{d}^*)^2}\right) \\ \vartheta_A^* &= \text{atan2}(\alpha_1^*, \alpha_3^*),\end{aligned}$$

where $\alpha^* = \mathbf{P}_L^* \mathbf{z}_S$ and \mathbf{P}_L^* is computed as in Sect. 4.4.2 from \mathbf{d}^* .

Notice that the equality $\mathbf{y}^b(t_L) = \mathbf{y}^{b*} = [\varphi^* \ \delta^* \ \vartheta_A^* \ \psi^*]^\top$, does not necessarily imply that $\mathbf{z}_R(t_L) = \mathbf{z}_R^*$. Indeed, controlling ϑ_A we control only the direction of the projection of \mathbf{z}_R on the plane \mathcal{P}_L . Whereas, the remaining component $\mathbf{y}_L^\top \mathbf{z}_R$ is not directly controlled but, for the flatness, it is given by the particular trajectory $\mathbf{y}^b(t)$ and its derivatives. A possible solution consists on planning a proper trajectory $\mathbf{y}^b(t)$ such that $\mathbf{y}^b(t_L) = \mathbf{y}^{b*}$ and $\mathbf{y}_L^\top \mathbf{z}_R(t_L) = \mathbf{y}_L^\top \mathbf{z}_R^* = 0$. Though, this technique based on motion planning shows the same drawbacks saw in Sect. 6.4 for the contact-free flight method.

However, for the case of interest when all the objectives of Sect. 6.3 are fulfilled and in particular Condition (4), a planner is not necessary. In this case, from Eq. (6.12) and the parametrization of \mathbf{d} , it is easy to see that $\mathbf{d}^* = \tilde{\mathbf{d}}$ implies $\delta^* = 0$. Finally, thanks to the flatness, we can demonstrate that if δ is stabilized to zero, i.e., $[\delta, \dot{\delta}, \ddot{\delta}] = \mathbf{0}$, then $\mathbf{y}_L^\top \mathbf{z}_R$ is stabilized to the desired value $\mathbf{y}_L^\top \mathbf{z}_R^* = 0$. Let us project (6.4) on \mathbf{y}_L considering $[\delta, \dot{\delta}, \ddot{\delta}] = \mathbf{0}$. We obtain:

$$-f_R \mathbf{y}_L^\top \mathbf{z}_R = \mathbf{y}_L^\top \mathbf{R}_A \left[l m_R \left(\begin{bmatrix} -c_\varphi \\ 0 \\ s_\varphi \end{bmatrix} \dot{\varphi} - \begin{bmatrix} s_\varphi \\ 0 \\ c_\varphi \end{bmatrix} \ddot{\varphi} \right) + f_L \begin{bmatrix} c_\varphi \\ 0 \\ s_\varphi \end{bmatrix} \right] + m_R g \mathbf{y}_L^\top \mathbf{z}_W. \quad (6.17)$$

Noticing that $\mathbf{y}_L^\top \mathbf{R}_A = \mathbf{e}_2^\top$ and $\mathbf{y}_L^\top \mathbf{z}_W = 0$, it is clear that $\mathbf{y}_L^\top \mathbf{z}_R = 0$.

This proves that, if \mathbf{p}_A is chosen such that $\mathbf{p}_L^* = \tilde{\mathbf{p}}_L$, then steering \mathbf{y}^b to \mathbf{y}^{b*} is sufficient to steer \mathbf{p}_{RL} and \mathbf{z}_R to \mathbf{p}_L^* and \mathbf{z}_R^* , respectively. In principle, we could generate a simple sufficiently smooth trajectory (like a spline) $\mathbf{y}^{bd}(t)$ from the initial output value to \mathbf{y}^{b*} that fulfill all the objectives of Sect. 6.3, and then track it with one of the controllers presented in Sects. 4.5.2 and 4.6.2, without the use of a planner. This makes the method more robust to tracking errors since they can be recovered by the controller avoiding the failure of the maneuver.

However, although not necessary, we still propose an optimal planner to more intuitively generate a desired trajectory that fulfills the conditions in Sect. 6.3, respecting the dynamics of the system, its input limits and other additional features in order to obtain an even more safe and reliable landing maneuver.

6.5.2 Optimal Planner

The computation of an optimal desired trajectory that fulfills the conditions of Sect. 6.3 can be formulated as an optimal control problem. Given the tethered system, we face a challenging nonlinear optimal control problem in a five dimensional configuration space. Even for a numerical solver it could be not easy to find a solution of this problem and its computation could require a lot of time. A common technique consists of simplifying the model of the system to make the problem solvable in a reasonable amount of time.

According to this method we assume⁴ $\delta(t) = 0$ for all $t \in [t_0, t_L]$. In practice this fact limits the motion of the vehicle on the 2D vertical plane $\mathcal{P}_M = \{\mathbf{x}_A, \mathbf{z}_A\}$, reducing the configuration space to two dimensions. This is not a problem since we showed that if δ converges to zero then also $\mathbf{y}_L^\top \mathbf{z}_R$ converges to $\mathbf{y}_L^\top \mathbf{z}_R^* = 0$. For simplicity we also assume a constant rotation around \mathbf{z}_R , i.e., $\psi(t) = \psi^*$ for all $t \in [t_0, t_L]$. This means that the system, while moving on \mathcal{P}_M , is fully described only by φ and ϑ_A , equivalently to the reduced model presented in Sect. 4.3 (indeed, $\vartheta_A = \theta$). We define $\mathbf{x}_M = [x_{M1} \ x_{M2} \ x_{M3} \ x_{M4}]^\top = [\varphi \ \vartheta_A \ \dot{\varphi} \ \dot{\vartheta}_A]^\top$ and $\mathbf{u}_M = [f_R \ \tau_{Ry}^A]^\top$ the state and input of the 2D system, respectively. In particular $\tau_{Ry}^A \in \mathbb{R}$ is the torque applied by the robot along the axis \mathbf{y}_A , i.e., $\tau_{Ry}^A = \mathbf{y}_A^\top \mathbf{R}_R \boldsymbol{\tau}_R$. Considering δ , \mathbf{y}_A^\top and their derivatives to zero, the dynamics can be derived as done in Sect. 4.8

$$\begin{bmatrix} \ddot{\varphi} \\ \ddot{\vartheta}_A \end{bmatrix} = \begin{bmatrix} a_1 \cos \varphi + a_2 \cos(\varphi + \vartheta_A) f_R \\ a_3 \tau_{Ry}^A \end{bmatrix} =: \mathbf{f}_M(\mathbf{x}_M, \mathbf{u}_M) \quad (6.18)$$

where $a_1 = -g/l$, $a_2 = 1/(m_R l)$, $a_3 = 1/(\mathbf{y}_A^\top \mathbf{R}_R \mathbf{J}_R)$.

⁴This can be guaranteed by the controllers proposed in Sects. 4.5.2 and 4.6.2.

From now on we focus on the generation of trajectories for a quadrotor-like VTOL since this is the robot used for the real experiments⁵ described in Sect. 6.6. As recalled in Sects. 3.2 and 3.3, this particular vehicle is equipped with four propellers, placed in a symmetric configuration with respect to the center of gravity, each one generating a thrust $f_i \in [\underline{f}_i, \bar{f}_i]$. All together the propellers generate the total thrust f_R and torque $\boldsymbol{\tau}_R$ applied to the vehicle according the relation $\mathbf{u} = [f_R \ \boldsymbol{\tau}_R]^\top = \Gamma \mathbf{u}_f$ where $\mathbf{u}_f = [f_1 \ f_2 \ f_3 \ f_4]^\top$ and $\Gamma \in \mathbb{R}^{4 \times 4}$ is a matrix that maps \mathbf{u}_f into \mathbf{u} (see Sect. 3.3.1). The matrix Γ depends on the parameters of the vehicle. We can then express \mathbf{u}_M as function of \mathbf{u}_f as

$$\mathbf{u}_M = \begin{bmatrix} 1 & \mathbf{0} \\ 0 & \mathbf{y}_A^\top \mathbf{R}_R \end{bmatrix} \Gamma \mathbf{u}_f = \Gamma_M \mathbf{u}_f. \quad (6.19)$$

Notice that Γ_M is constant since, given the constraint of moving on \mathcal{P}_M , the vehicle body rotates only around \mathbf{y}_A . Then, replacing (6.19) into (6.18) we can define $\mathbf{f}_{Mf}(\mathbf{x}_M, \mathbf{u}_f) = \mathbf{f}_M(\mathbf{x}_M, \Gamma_M \mathbf{u}_f)$.

It is well known that the propellers of a real quadrotor can not immediately actuate a commanded thrust and that the time response depends on the particular motors and propellers. In order to obtain a feasible and smoother trajectory for the system we decided to consider a double dynamic extension of the model assuming as new input the second derivative of the thrust, $\bar{\mathbf{u}}_f = [\ddot{f}_1 \ \dots \ \ddot{f}_4]^\top$. The new extended state becomes $\bar{\mathbf{x}}_M = [\varphi \ \vartheta_A \ \dot{\varphi} \ \dot{\vartheta}_A \ \ddot{\varphi} \ \ddot{\vartheta}_A \ \varphi^{(3)} \ \vartheta_A^{(3)} \ \mathbf{u}_f^\top \ \dot{\mathbf{u}}_f^\top]^\top$. The dynamics becomes

$$\dot{\bar{\mathbf{x}}}_M = \begin{bmatrix} \mathbf{0} & \mathbf{I}_6 & \mathbf{0} & \mathbf{0} \\ \mathbf{0} & \mathbf{0} & \mathbf{0} & \mathbf{0} \\ \mathbf{0} & \mathbf{0} & \mathbf{I}_4 & \mathbf{0} \\ \mathbf{0} & \mathbf{0} & \mathbf{0} & \mathbf{0} \end{bmatrix} \bar{\mathbf{x}}_M + \begin{bmatrix} \mathbf{0} \\ \ddot{\mathbf{f}}_{Mf}(\bar{\mathbf{x}}_M, \bar{\mathbf{u}}_f) \\ \mathbf{0} \\ \bar{\mathbf{u}}_f \end{bmatrix} = \bar{\mathbf{f}}_{Mf}(\bar{\mathbf{x}}_M, \bar{\mathbf{u}}_f). \quad (6.20)$$

We highlight the fact that for a very reactive vehicle characterized, e.g., by a low mass and inertia, this dynamic extension could be avoided, since it would be able to actuate fast varying inputs. Nevertheless, this allows us to generate a C^3 trajectory required by Γ_{DFL}^b .

Given the system dynamics (6.20), we are ready to formalize our optimal control problem as

$$\begin{aligned} & \min_{\bar{\mathbf{x}}_M(t), \bar{\mathbf{u}}_f(t)} J(\bar{\mathbf{x}}_M(t), \bar{\mathbf{u}}_f(t), t, t_L) \\ & \text{subject to, } \forall t \in [t_0, t_L] \\ & (a) \ \dot{\bar{\mathbf{x}}}_M = \bar{\mathbf{f}}_{Mf}(\bar{\mathbf{x}}_M(t), \bar{\mathbf{u}}_f(t)) \quad (b) \ \bar{\mathbf{x}}_M(t_0) = \bar{\mathbf{x}}_{M0} \\ & (c) \ \underline{f}_i \leq f_i(t) \leq \bar{f}_i \quad (d) \ f_L(t) > 0 \end{aligned} \quad (6.21)$$

⁵The method can be easily modified according to any VTOL.

where $J : \bar{\mathbf{x}}_M, \bar{\mathbf{u}}_f \rightarrow \mathbb{R}$ is the cost function, (a) is the dynamics, (b) are the initial conditions, (c) are the input limits, and (d) prevents the link to become slack. In order to fulfill the objectives of Sect. 6.3, we define the cost function as:

$$J = \int_{t_0}^{t_L} (J_1 + J_2 + J_3 + J_4) d\tau + J_5$$

where

$$J_1 = k_\varphi (\varphi - \varphi^*)^2 + k_{\vartheta_A} (\vartheta_A - \vartheta_A^*)^2 + k_{\dot{\varphi}} \dot{\varphi}^2 + k_{\dot{\vartheta}_A} \dot{\vartheta}_A^2 + k_{\ddot{\varphi}} \ddot{\varphi}^2 + k_{\ddot{\vartheta}_A} \ddot{\vartheta}_A^2$$

$$J_2 = k_{\vartheta_A 2} h_{\vartheta_A}(\varphi) (\vartheta_A - \vartheta_A^*)^2$$

$$J_3 = k_{\dot{\varphi} \dot{\vartheta}_A} h_{\dot{\varphi} \dot{\vartheta}_A}(\varphi) (\dot{\varphi}^2 + \dot{\vartheta}_A^2)$$

$$J_4 = k_{\bar{\mathbf{u}}_f} \bar{\mathbf{u}}_f^2$$

$$J_5 = k_{t_L \vartheta_A} \dot{\vartheta}_A^2 + k_{t_L \dot{\varphi}} \dot{\varphi}^2$$

and $k_\star \in \mathbb{R}_{\geq 0}$, $h_{\vartheta_A}(\varphi)$ and $h_{\dot{\varphi} \dot{\vartheta}_A}(\varphi)$ are functions that tend to 1 when φ is near φ^* , and to zero otherwise. The cost terms 1, 3, 5 together, help to fulfill the conditions of Sect. 6.3, i.e., to steer the vehicle on the surface approaching it with zero velocities and accelerations. The cost term 2 enforces to approach \mathcal{P}_S with the proper attitude, such that the landers touch the surface simultaneously. Finally, the cost term 4 avoids fast variations on the commanded thrust that otherwise could not be actuated. Modifying the gains of J one can adjust the trajectory to obtain different behaviors.

The solution of the optimal control problem, $\bar{\mathbf{x}}_M^d(t)$ for $t \in [t_0, t_L]$, is computed using the ACADO [9] numerical optimizer. Finally, $\bar{\mathbf{x}}_M^d(t)$ together with $\delta^d(t) = 0$ and $\psi^d(t) = \psi^*$ give the desired output trajectory $\mathbf{y}^{bd}(t)$ to be tracked in order to perform the landing.

6.6 Experimental Landing and Takeoff

In this section we show the main results of the experiments that validate the efficacy of our proposed method for the problem of landing (and takeoff) on a sloped surface.

In particular, we consider the plausible scenario where a quadrotor-like vehicle has to deploy a smaller robot or a sensor on a sloped surface tilted by 50° , shown in Fig. 6.4. The robot, equipped with a cable ending with a hook, starts from a non-tethered configuration on the ground. Therefore it has to anchor the other end of the cable to the surface to then perform the landing in a tethered configuration. Once the robot has landed on the desired spot and deployed the robot/sensor, it can takeoff from the surface again exploiting the tether. Finally it can go back to the initial position after having detached the cable from the surface. The hardware employed for the experiment is the one described in Sect. 5.1.2.

Fig. 6.2 Zoom of the hook and the anchoring mechanism



6.6.1 Anchoring Tools and Mechanisms

In order to pass from a contact-free flight configuration to a tethered one, a method to fix the end of the cable to the surface has to be found. The mechanism to do so strongly depends on the application scenario and in particular on the material of the slope. For example, in the context of the European project *Aeroarms*,⁶ an aerial robot has to deploy a magnetic crawler or a sensor on industrial pipes that are often non-horizontal. In this context the landing surface is mainly a pipe made of iron/steel. Thus in this case, and whenever the surface is made of proper metal, a magnetic anchor can be used to enhance the physical connection between surface and the robot. In the case of a ground, snowed, or iced surface an harpoon-like mechanism might be envisaged.

In our experimental testbed we instead used a simpler solution based on a commercial fishing hook made of three tips, and an anchoring mechanism fixed to the surface made by a horizontal cable. In this way the robot can be tethered to the surface by sliding the vertical cable on the anchoring mechanism until the hook is anchored to the horizontal cable, as shown in Fig. 6.2. The hook can be detached from the anchoring mechanism doing the opposite operation.

6.6.2 Experimental Phases

Considering the previous experimental scenario and the goal, we divided the overall maneuver into several phases:

- (a) approach to the anchor point with the hook,
- (b) hooking of the anchoring system,
- (c) stretching of the cable,
- (d) tracking of the desired trajectory for tethered landing.

The phases from (a) to (c), described by the first row of images in Fig. 6.4, serve to pass from the initial contact-free flight configuration to the tethered one. Using a

⁶<http://www.aeroarms-project.eu/>.

standard contact-free flight position controller and following a straight-line trajectory, the robot is able to anchor the anchoring system attached to the surface with the hook (see Fig. 6.4b.2). The trajectory is planned such that the cable attached to the robot slides on the anchoring cable until the hook results attached to the last one.

Afterward, during phase (c), the cable is stretched following a simple radial trajectory whose ending point is slightly outside the reachable region limited by the cable length. The robot, trying to reach this ending position, as explained in [10], will apply an extra force to the cable that will make it taut. In particular, the farther the desired ending position, the larger the internal force on the link. Using the dynamics of the system, the estimated state, and the control inputs, the robot can estimate the tension on the link. This estimation is then used to understand when the cable results sufficiently taut. Once the tension exceeds a certain security threshold a supervisor switches from the contact-free flight controller to the tethered one. We recall that for this experiment we use the hierarchical controller Γ_{HC}^b presented in Sect. 4.5.2 whose validity has been experimentally demonstrated in Sect. 5.2. In fact, Γ_{HC}^b can guarantee sufficiently small tracking errors for the slow trajectories needed for the safety of the maneuvers. This additionally shows that the tethered solution does not require a very precise tracker.

Finally the planned landing trajectory is tracked. In order to compute the desired landing and takeoff trajectories using the planner presented in Sect. 6.5, the parameters of the landing surface, such as slope angle and anchoring point, must be known. To acquire those values we applied some markers on the surface to measure its pose with a motion capture system. However, thanks to the robustness of the method, those parameters does not have to be very precise.

Once the robot ends the landing maneuver the takeoff can start. The takeoff maneuver is very similar to the play-back of the previous phases. Indeed, following the previous trajectory in the opposite sense lets the hook be detached from the anchoring mechanism to then go back to the starting point in a contact-free flight configuration.

6.6.3 Controller Switch

During the switching between the controllers, the continuity of the control input has to be guaranteed in order to preserve the stability of the system and to avoid undesired vibrations and jerks on the cable. This is obtained by setting as desired output of the next controller, the value of the system output at the switching instant. This is possible because, thanks to the flatness, there is a bijective relation between state/input and output. Therefore, for a specific output, there exist a unique nominal input and state to obtain it. Assume that the system is in a certain state with a certain input, \mathbf{x}_0 and \mathbf{u}_0 , respectively. Accordingly we have a particular output value \mathbf{y}_0 . Asking the next controller to keep the output value \mathbf{y}_0 we will obtain the same input \mathbf{u}_0 and state \mathbf{x}_0 , thus preserving the continuity of the control action and of the full state.

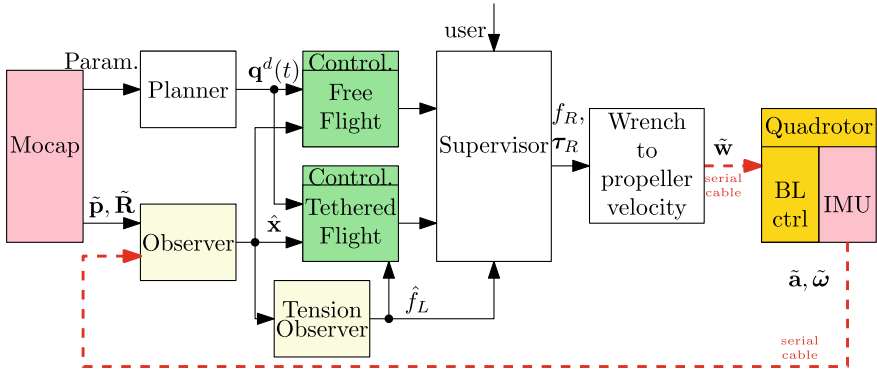


Fig. 6.3 Schematic representation of the software architecture. Pink blocks represent the sensors. Green blocks represent the controllers and light yellow blocks represent the observers. Starting from the left, $\tilde{\mathbf{p}}$ and $\tilde{\mathbf{R}}$ represent the measured robot position and orientation, respectively; $\hat{\mathbf{x}}$ and \hat{f}_L represent the estimated state and link internal force, respectively; $\mathbf{q}^d(t)$ represents the desired output trajectory; f_R and $\boldsymbol{\tau}_R$ represents the input of the robot, i.e., thrust intensity and torque vector; $\tilde{\boldsymbol{\omega}}$ represents the desired spinning velocity of the propellers. Finally $\tilde{\mathbf{a}}$ and $\tilde{\boldsymbol{\omega}}$ represent the readings of the IMU, i.e., specific acceleration and angular velocity

6.6.4 Software Architecture

A schematic representation of the software architecture is represented in Fig. 6.3. The overall controllers and observers run on a ground PC. The desired spinning velocities of each propeller are sent at 500 Hz to the robot using a serial cable. The received velocity commands are then actuated by a controller (presented in [11]) running on the on-board ESC (Electronic Speed Control). The same serial communication is used to read at 1 KHz the IMU measurements that are then UKF-fused together with the motion capture system measurements (position and orientation of the quadrotor at 120 Hz) to obtain an estimation of the state of the vehicle. The latter is then used to close the control loop and to compute an estimation of the internal force along the link when it is taut.

The controller for the contact-free flight and tethered cases run in parallel and a supervisor, according to the state of the experiment, decides whose input has to be applied to the real system. The user input in the supervisor is needed to trigger situations of emergency.

6.6.5 Offset Nonideality

Another practical aspect that has to be considered is the nonzero offset between the cable attaching point and the vehicle center of mass. Indeed, the controller Γ_{HC}^b presented in Sect. 4.5.2 assumes that this offset is equal to zero. In this way the

robot translational and rotational dynamics can be decoupled. However, this never happens in a practical case. Then, due to this non-zero offset, the internal force along the cable generates a torque on the vehicle that has to be carefully compensated. This is done computing the extra torque from the estimated tension and the estimated offset calculated with a mechanical analysis.

Finally we highlight the fact that the maximum tilting of the surface is bounded by the input limits. Indeed the more inclined is the slope, the less it is the thrust required to compensate the gravity close to the surface. Due to the impossibility of producing negative thrust for the single propeller, the almost zero total thrust implies a reduced control authority on the total input moment that may cause the instability of the attitude dynamics and of the whole system in general.

6.6.6 Experimental Results

In Figs. 6.4 and 6.5 the experimental results are shown. In this particular case the robot has to land and then takeoff on/from a planar surface that is tilted by 50° . Figure 6.4 shows the first half of the experiment, i.e., the landing, by a series of images. In particular the first row shows the anchoring procedure done in a contact-free flight condition. On the other hand, the second row shows the actual execution of the tethered landing. A video of the full experiment is available at [12].

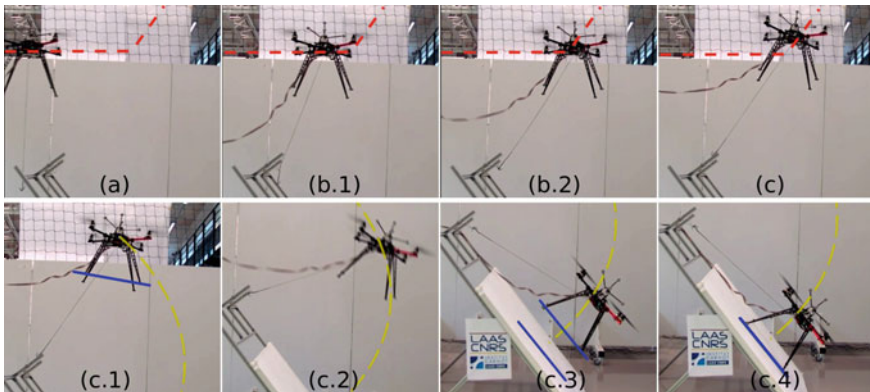


Fig. 6.4 Sequence of images of a real experiment with a sloped surface tilted by 50° . The first row of images represents the experimental part in which the quadrotor is in a contact-free flight condition. In this case a standard position controller is used to track the desired position trajectory marked with a dashed red line. The second row of images represents the experimental part in which the quadrotor is tethered to the surface. In this case the controller proposed in Sect. 4.5.2 is used to track the desired position and attitude trajectories marked with a dashed yellow line and a solid blue line, respectively

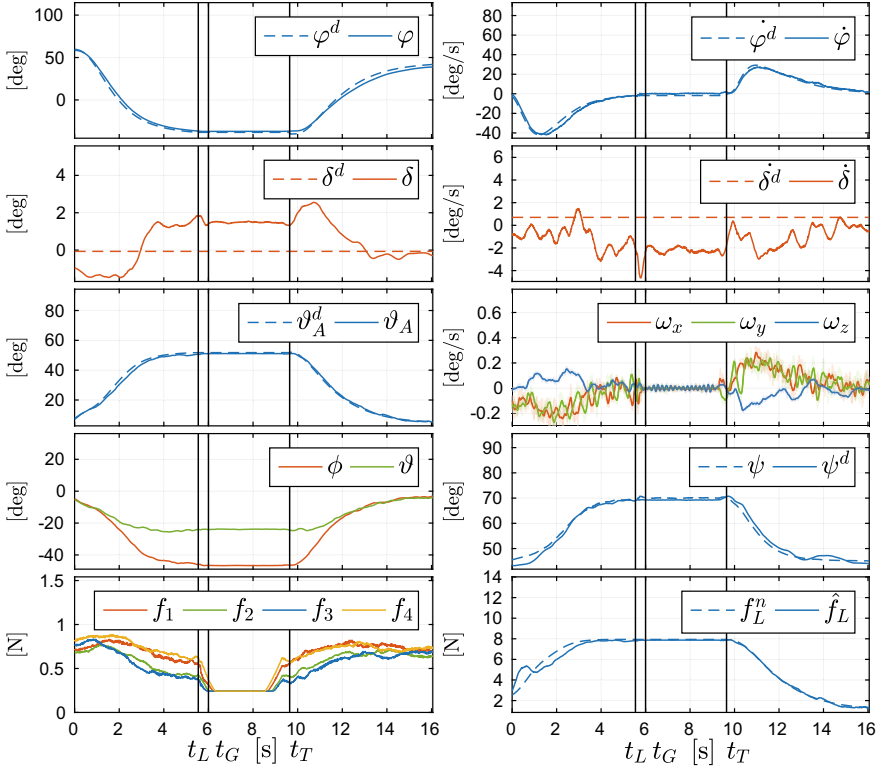


Fig. 6.5 Experimental results: plots of the state, outputs and inputs of the system during the tethered landing and takeoff. In particular φ and δ describe the attitude of the cable and, given the link constraint, the position of the vehicle with respect to the anchoring point. ϕ and ψ are the angles that together with ϑ_A describe the orientation of the robot. f_1, f_2, f_3, f_4 are the forces produced by each propeller. Finally, f_L is the intensity of the internal force along the link. The super-script d and n represent the desired and the nominal values of a variable, respectively

Figure 6.5 shows the evolution of the state, outputs and inputs of the system during the landing and takeoff maneuvers. At time zero the tethered controller is activated and the landing maneuver starts. At time t_L the landing is accomplished and the surface is reached. At time t_G the motors are stop to simulate the deploying of a robot/sensor. Finally, at time t_T the takeoff maneuver starts.

From those plots one can see that the desired trajectory is tracked precisely, with only some small errors due to calibration inaccuracy. Furthermore, notice that the intensity of the internal force is always positive. This shows that the cable is kept taut for the whole execution of the maneuvers. Despite the presence of tracking errors the landing and takeoff maneuver are accomplished successfully and in a very safe and gentle way. This shows the big advantage of using a tether that makes the execution

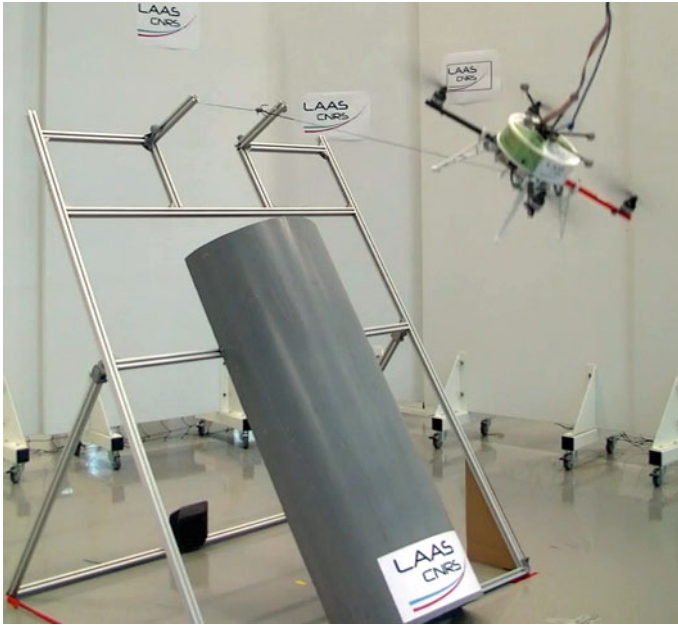


Fig. 6.6 Execution of a tethered landing on an inclined pipe tilted by 60°

on the task reliable and robust to tracking and modeling errors. Thanks to this we were able to perform landing and takeoff on/from an even non-flat surface (a pipe) tilted up to 60° . We provide an image from such experiment in Fig. 6.6.

References

1. Cabecinhas, D., Naldi, R., Marconi, L., Silvestre, C., Cunha, R.: Robust take-off for a quadrotor vehicle. *IEEE Trans. Robot.* **28**(3), 734–742 (2012)
2. Mellinger, D., Michael, N., Kumar, V.: Trajectory generation and control for precise aggressive maneuvers with quadrotors. *Int. J. Robot. Res.* **31**(5), 664–674 (2012)
3. Mueller, M.W., Hehn, M., D’Andrea, R.: A computationally efficient algorithm for state-to-state quadcopter trajectory generation and feasibility verification. In: 2013 IEEE/RSJ International Conference on Intelligent Robots and Systems, pp. 3480–3486, Tokyo, Japan (2013)
4. Martin, P., Devasia, S., Paden, B.: A different look at output tracking: control of a VTOL aircraft. *Automatica* **32**(1), 101–107 (1996)
5. Tognon, M., Testa, A., Rossi, E., Franchi, A.: Takeoff and landing on slopes via inclined hovering with a tethered aerial robot. In: 2016 IEEE/RSJ International Conference on Intelligent Robots and Systems, pp. 1702–1707, Daejeon, South Korea (2016)
6. Tognon, M., Franchi, A.: Landing and take-off on/from sloped and non-planar surfaces with more than 50 degrees of inclination. In: 9th International Micro Air Vehicles Conference, pp. 97–102 (2017)

7. Faessler, M., Franchi, A., Scaramuzza, D.: Differential flatness of quadrotor dynamics subject to rotor drag for accurate tracking of high-speed trajectories. *IEEE Robot. Autom. Lett.* **3**(2), 620–626 (2018)
8. Mohta, K., Kumar, V., Daniilidis, K.: Vision-based control of a quadrotor for perching on lines. In: 2014 IEEE International Conference on Robotics and Automation, pp. 3130–3136 (2014)
9. Houska, B., Ferreau, H., Diehl, M.: ACADO Toolkit - an open source framework for automatic control and dynamic optimization. *Opt. Control Appl. Methods* **32**(3), 298–312 (2011)
10. Gioioso, G., Ryll, M., Prattichizzo, D., Bühlhoff, H.H., Franchi, A.: Turning a near-hovering controlled quadrotor into a 3D force effector. In: 2014 IEEE International Conference on Robotics and Automation, pp. 6278–6284, Hong Kong, China (2014)
11. Franchi, A., Mallet, A.: Adaptive closed-loop speed control of BLDC motors with applications to multi-rotor aerial vehicles. In: 2017 IEEE International Conference on Robotics and Automation, pp. 5203–5208, Singapore (2017)
12. video 1: Takeoff and landing on slopes via inclined hovering with a tethered aerial robot. <https://www.youtube.com/watch?v=01UYN289YXk> (2016)